

Diagnosing GCM errors over West Africa using relaxation experiments. Part I: summer monsoon climatology and interannual variability

Benjamin Pohl · Hervé Douville

Received: 9 February 2010 / Accepted: 10 September 2010
© Springer-Verlag 2010

Abstract The CNRM atmospheric general circulation model Arpege-Climat is relaxed towards atmospheric reanalyses outside the 10°S–32°N 30°W–50°E domain in order to disentangle the regional versus large-scale sources of climatological biases and interannual variability of the West African monsoon (WAM). On the one hand, the main climatological features of the monsoon, including the spatial distribution of summer precipitation, are only weakly improved by the nudging, thereby suggesting the regional origin of the Arpege-Climat biases. On the other hand, the nudging technique is relatively efficient to control the interannual variability of the WAM dynamics, though the impact on rainfall variability is less clear. Additional sensitivity experiments focusing on the strong 1994 summer monsoon suggest that the weak sensitivity of the model biases is not an artifact of the nudging design, but the evidence that regional physical processes are the main limiting factors for a realistic simulation of monsoon circulation and precipitation in the Arpege-Climat model. Sensitivity experiments to soil moisture boundary conditions are also conducted and highlight the relevance of land–atmosphere coupling for the amplification of precipitation biases. Nevertheless, the land surface hydrology is not the main explanation for the model errors that are rather due to deficiencies in the atmospheric physics. The

intraseasonal timescale and the model internal variability are discussed in a companion paper.

Keywords West African monsoon · AMMA · Climate modeling · Grid-point nudging

1 Introduction

The West African monsoon climate shows strong variability on a wide range of timescales. Understanding and, ultimately, predicting the onset of the monsoon season, the year-to-year variability in summer precipitation and the multi-decadal evolution of the monsoon are key challenges for the climate modeling community. Unfortunately, state-of-the-art seasonal predictions (e.g. Garric et al. 2002; Bouali et al. 2008) and climate change projections (e.g. Douville et al. 2006; Biasutti et al. 2009) based on coupled ocean–atmosphere General Circulation Models (GCM) are still very uncertain. Such results might be partly explained by the limited ability of the coupled models even to capture the mean seasonal climate over West Africa. Many models do not place the monsoon precipitation maximum over the African land surface, but over the Gulf of Guinea to the south of the coast (e.g. Cook and Vizy 2006). They also fail in capturing the high-frequency atmospheric variability (Ruti and Dell’ Aquila 2008) and the teleconnections with tropical sea surface temperature (SST) at interannual timescale (Joly et al. 2007). Even when driven by prescribed SST, many atmospheric GCMs do not simulate properly the seasonal and intraseasonal features of the monsoon and there is apparently no simple relationship between the biases at different timescales (e.g. Sperber and Palmer 1996; Moron et al. 2004; Hourdin and The AMMA-MIP team 2010). This is not so surprising given the lack of

B. Pohl · H. Douville
CNRM/GAME, Météo-France/CNRS, Toulouse, France

B. Pohl (✉)
Centre de Recherches de Climatologie,
CNRS/Université de Bourgogne,
6 Boulevard Gabriel, 21000 Dijon, France
e-mail: benjamin.pohl@u-bourgogne.fr

consensus about the role of scale interactions over West Africa (Leroux and Hall 2009; Pohl et al. 2009).

In the framework of the AMMA program (African Monsoon Multidisciplinary Analysis: <http://amma-international.org/>) and of the IRCAAM project (Influence Réciproque des Climats de l'Afrique de l'Ouest, du sud de l'Asie et du bassin Méditerranéen: <http://www.cnrm.meteo.fr/ircaam/>) funded by the French National Research Agency, the main objective of the present study is to evaluate and better understand the systematic errors of the Arpege-Climat atmospheric GCM over West Africa. Despite its noteworthy behavior in the AMMA-MIP intercomparison project (Hourdin and The AMMA-MIP team 2010), the model shows marked regional biases during the summer monsoon season, even when driven by observed SST. Rainfall amounts over the Sahel are too low and the monsoon flow remains far too weak, especially over the equatorial Atlantic basin (Bielli et al. 2010, B10 hereafter). In order to improve our understanding of the model biases, we use the so-called grid-point nudging technique (Douville 2009; Jung et al. 2009, B10) to relax the model towards 6-hourly atmospheric reanalyses outside of the West African monsoon domain.

This diagnostic technique allows us to disentangle the remote versus regional influences on the monsoon simulation. It differs from the well-known regional climate model (RCM) approach (e.g. Vanvyve et al. 2008; Separovic et al. 2008; Sylla et al. 2010) in several ways. First, the horizontal resolution is not increased over West Africa compared to the control (i.e. free) global atmospheric simulation. While the nudging technique can also be used as a dynamical downscaling tool (e.g. Yoshimura and Kanamitsu 2008), the aim here is not to analyze whether the model biases are sensitive to the resolution, but to address their regional versus remote origin. Second, the nudging technique avoids many technical issues related to the treatment of lateral boundary conditions in limited area models (Leung et al. 2003). Ideally, one should specify the inflow boundary and use an open outflow boundary to reduce numerical errors. In practical terms, this is not possible and the design of RCM experiments is relatively tricky, involving horizontal and vertical interpolation of the large-scale forcing on the model grid, the use of sponge or simple nudging techniques near the lateral boundaries for avoiding undesirable conflicts between large-scale forcing and internal variability (i.e. the irreproducible component of the RCM integrations), and possibly the use of large-scale spectral nudging within the regional domain for a stronger control on such internal variability (e.g. Alexandru et al. 2009). On the one hand, the nudging technique used in the present study shares some of the RCM technical issues, such as a possible sensitivity to the domain size and location. On the other hand, it is a more flexible tool. There

is neither jump in horizontal resolution, nor need of vertical interpolation at the lateral boundaries. The strength of the nudging can be varied in space (x, y, z) and is not necessarily the same for all prognostic variables. The relaxation reference fields, here derived from 6-hourly reanalyses interpolated at the model time step, can be filtered so that the nudging technique can also be very useful to study scale interactions.

The study is organized as follows. The experimental design is detailed in Sect. 2. Section 3 evaluates the model biases and the impact of nudging based on a series of AMIP-type experiments driven by observed monthly mean SST over the 1971–2000 period. Besides seasonal mean errors, it also briefly describes the impact of nudging on interannual variability. Section 4 selects summer 1994 as a representative case study and conduct several sensitivity tests to further understand the possible reasons for the model biases and their relative resistance to the relaxation technique. Each test consists of a 30-member ensemble of seasonal simulations driven by the observed 1994 monthly mean SST. Besides the sensitivity to the strength of the nudging and/or to the filtering of the relaxation fields, the role of lateral and soil moisture boundary conditions is also explored. The results are summarized and further discussed in Sect. 4.

2 Data and experimental design

All simulations are based on version 4 of the Arpege-Climat model, derived from the Arpege/IFS numerical weather prediction model developed jointly by the European Centre for Medium-range Weather Forecasts (ECMWF) and Météo-France. It is a spectral model with a progressive hybrid σ -pressure vertical coordinate. The model is used in its standard configuration (linear T63 truncation, reduced 128×64 Gaussian grid, 31 vertical levels). The dynamical core uses a semi-implicit, semi-Lagrangian, two-time level discretization scheme. The physical package is partly inherited from the Météo-France operational weather forecast model and is very similar to the one used by CNRM in the CMIP3 simulations (Salas y Méria et al. 2005). In particular, it includes a mass flux convective scheme with a Kuo-type closure (Bougeault 1985) and a two-layer force-restore soil hydrology (Noilhan and Planton 1989).

The nudging protocol used here is similar to that already used in B10. The 6-hourly ECMWF reanalyses (ERA40, Uppala et al. 2005) have been used as a reference to prescribe the tropical atmosphere in the nudged experiments. The nudging is applied on each time step t_{step} (with $t_{\text{step}} = 30$ min here), to the zonal and meridional wind components, temperature, specific humidity and sea-level

pressure. This is done by adding a $-\lambda(y - y_{\text{ref}})$ term in the model prognostic equations, where y is the model state vector, y_{ref} the reference field towards which the model is relaxed, and $\lambda = t_{\text{step}}/e_{\text{time}}$ is the strength of the relaxation, with e_{time} the e-folding relaxation time (fixed here at 5 h for U and V, i.e. $\lambda = 0.1$, against 12 h for the other variables, i.e. $\lambda = 0.04$). The nudging is also weaker at the three lowest and five highest levels, in order to let the model adjust to the nudging and/or perturbed surface boundary conditions (such as prescribed SST or total soil moisture).

Although Arpege-Climat is a spectral atmospheric model, the nudging is here achieved on a limited 3D domain and therefore on the Gaussian grid, after an inverse spectral transform. The nudging is applied outside the domain $10^{\circ}\text{S}-32^{\circ}\text{N}$ $30^{\circ}\text{W}-50^{\circ}\text{E}$ (Fig. 1), with a 5° buffer zone in which the nudging vanishes progressively in order to ensure a relatively smooth transition between the nudged and free atmosphere. Sensitivity experiments to the domain size and the location of its bounds were also conducted (not shown). None of the results discussed below were shown to be qualitatively modified by the nudging domain.

The basic set of experiments is summarized in Table 1. The control experiment, FCI, is a 30-year simulation (after a 2-year spin-up) driven by the ERA40 monthly mean climatological SST averaged over the 1971–2000 period. It is used to obtain the model climatology and to provide initial conditions for all other integrations. A parallel 1971–2000 integration, FCt, has been performed using the observed ERA40 monthly mean SST, including their interannual variability. It is used to document the model seasonal mean state and its year-to-year variability.

All nudging experiments consist in ensembles of 30 boreal summer integrations initialized on May 15th from each of the individual year of FCI. Daily outputs have been archived from June 1st to September 30th (hereafter the JJAS season), i.e. after a 15-day spin-up allowing the

Arpege-Climat model to adjust to the nudging and/or the perturbed boundary conditions.

NCT is a nudged ensemble driven by the same SST forcing as FCt, that consists of 30 JJAS seasons over the 1971–2000 period. It is devoted to the analysis of the modifications of the model climatology due to the nudging, as well as to a preliminary assessment of its impact on the WAM interannual variability. The robustness of the results is questionable as they depend on a single 30-year interannual integration. In order to address this problem, we chose to focus on a given rainy season presenting large departures from the seasonal mean, and to compute ensembles of 30 members initialized with differing conditions derived from FCI experiment. We retained 1994 as a case study, as this year is the wettest of the period according to GPCP rainfall estimates over the Sahel (e.g. B10, see their Fig. 10).

F94 is a 30-member integration driven by the observed 1994 monthly mean SST field, without atmospheric nudging. N94 is nudged towards 1994 ERA40 fields and is driven by observed SST. In order to evaluate the effects of the grid-point nudging, n94 is similar to N94 except that the strength of the relaxation is divided by 10 (i.e. $\lambda = 0.01$ for U and V and $\lambda = 0.004$ for T, Q and MSLP). I94 is nudged towards the more recent and hopefully more reliable ERA-Interim re-analysis (Simmons et al. 2007) using the same protocol as in N94.

The four ensemble experiments NA94, nA94, NB94 and nB94 are devoted to the analysis of scale interactions. “A” experiments are nudged towards 9-day lowpass filtered ERA40 fields (computed to remove the synoptic-scale variability, and particularly that related to African Easterly Waves) and “B” experiments are nudged towards 25-day lowpass filtered fields in order to suppress the 10–25-day Sahelian mode (Sultan et al. 2003). Both strong (“N”) and weak (“n”) nudging strength protocols are used, in order to remove sub-synoptic variability from the lateral boundary conditions (“N” experiments), or to let the model simulate its own high-frequency variability within a guided background state (“n” experiments). FS94, NS94 and IS94 experiments were specifically designed to investigate the sensitivity to soil moisture and will be more extensively discussed and presented in Sect. 4.4.

Rainfall estimates are provided by the Global Precipitation Climatology Project dataset (GPCP, Huffman et al. 1997). They are available at the pentad (5-day) timescale on a worldwide $2.5^{\circ} \times 2.5^{\circ}$ regular grid. For consistency with the nudging fields, ERA40 precipitation fields are also considered, even if their reliability is highly questionable. Uncertainties associated with the choice of the rainfall estimates and consequences for the computation of the atmospheric water budget over West Africa are widely discussed in Meynadier et al. (2010a, b).

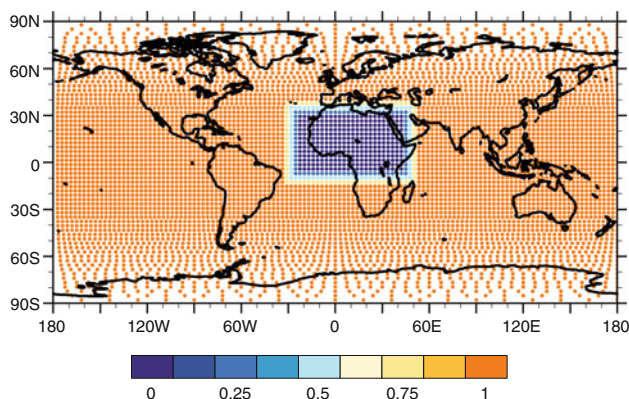


Fig. 1 Nudging mask, with a smooth transition between full (1) and no (0) nudging

Table 1 Summary of the interannual 1971–2000 and 30-member 1994 ensemble experiments conducted with the Arpege-Climat model over the JJAS season

	FCI [<i>CtCI</i>]	FCt [<i>CtIV</i>]	F94	NCt [<i>NAfNuIV</i>]	N94	n94	I94
Period	1971–2000	1971–2000	1994	1971–2000	1994		
Nudging	No			Strong		Weak	Strong
Nudging domain	–			Outside 10°S 32°N 30°W 50°E			
Nudging Fields	–			Unfiltered ERA40			Unfiltered ERA-Interim
Soil wetness	Interactive						
	NA94	nA94	NB94	nB94	FS94	NS94	IS94
Period	1994						
Nudging	Strong	Weak	Strong	Weak	No	Strong	
Nudging domain	Outside 10°S 32°N 30°W 50°E				–	Outside 10°S 32°N 30°W 50°E	
Nudging fields	9-day lowpass ERA40		25-day lowpass ERA40		–	Unfiltered ERA40	Unfiltered ERA-Interim
Soil wetness	Interactive				Nudged towards GSWP-2		

See text for details. Experiments already used in B10 were given their equivalent names (in italics)

3 Multi-year experiments

3.1 Summer mean climate

B10 showed that the model JJAS climatology over West Africa is only marginally modified by a quasi-global nudging. The location and intensity of the main features of the WAM (namely the lower-layer monsoon flow, the mid-tropospheric African Easterly Jet, AEJ, and the upper-layer Tropical Easterly Jet, TEJ) were little affected. Importantly, the dry biases over the Sahel were not reduced. Figures 2 and 3 aim at documenting the effects of the nudging on simulated rainfall and moisture fluxes and divergence over West Africa, in order to better understand the possible origin of such persisting biases (see Appendix for details on moisture flux computation).

ERA40 vertically integrated moisture fluxes (Fig. 2a) reveal the well-known pattern associated with the inter-tropical convergence over West Africa in boreal summer, and its northward shift due to radiative heating over the subcontinent. The monsoon flow itself is barely perceptible in the Gulf of Guinea, while the one associated with the Indian monsoon clearly appears in the east of the domain. Moisture fluxes reaching the Sahel mainly originate from the Gulf of Guinea (Mediterranean) in the southern (northern) meteorological hemisphere. Consistently with B10, the model biases over the Sahel mainly result of a too weak monsoon flow (Fig. 2c), which conveys too few moisture from the equatorial Atlantic. Symmetrically, moisture advection from the Mediterranean is also too weak, explaining the too low moisture convergence over the Sahel. These biases are not improved by the nudging (Fig. 2b–d), as confirmed by RMS statistics computed over the overall free (i.e. not nudged) domain. Moisture

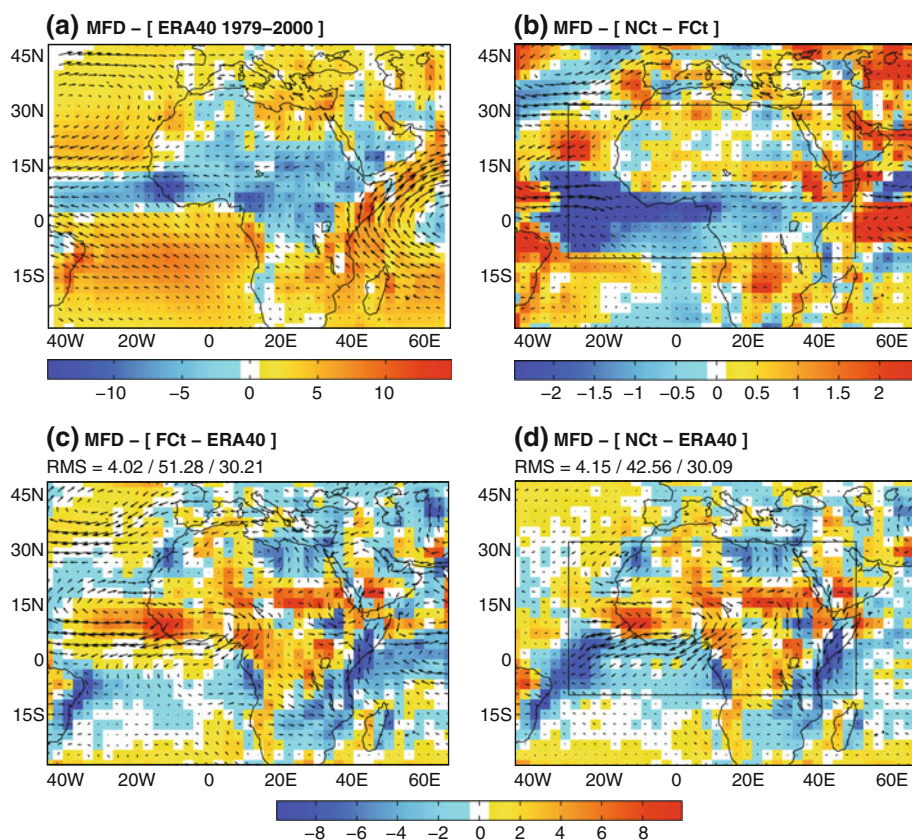
divergence is only reduced over the nearby Atlantic basin but is not modified over Africa.

As a consequence, simulated rainfall also presents marked deficiencies compared to GPCP estimates (Fig. 3). GPCP and ERA40 both place the rainfall maximum during the JJAS season over the African continent (Fig. 3a), but the ERA40 rainfall maximum is unrealistically shifted towards the South and rainfall amounts are generally too low. Compared to GPCP, Arpege-Climat shows marked dry biases over West Africa, contrasting with wet ones over the East African Highlands (Fig. 3c). In the free domain, the precipitation biases are not improved by the quasi-global nudging (Fig. 3d). An RMS statistics computed on all grid points in the free domain even indicates a deterioration by 9%. Spatially the impact of the nudging is not uniform (Fig. 3b) and the deterioration is mostly due to larger rainfall amounts over the equatorial Atlantic Ocean. Like most GCMs, Arpege-Climat presents wet biases over the Guinean Gulf, which are enhanced by the nudging. Comparisons with ERA40 precipitation however reveal a slight improvement of the model biases over West Africa (with an RMS decreased by 7% in NCt). Over the African continent, Arpege-Climat simulates lower (higher) rainfall amounts over the Guinean belt (the Sahel). The latitudinal extension of the WAM is thus more realistically simulated in Arpege-Climat than in ERA40. Rainfall amounts over East Africa remain nevertheless too high in both free and nudged experiments, in relationship with too high moisture convergence (Fig. 2c, d).

3.2 Interannual variability

Based on the same experimental design, B10 depict a clear improvement of the interannual variability of the WAM –in spite of a mean state barely affected, Sect. 3.1. Their results are based on a seasonal West African Monsoon Index

Fig. 2 **a** Vectors ERA40 vertically integrated moisture fluxes, period JJAS 1979–2000. Shading moisture divergence (mm day^{-1}), see legend for colour shading. **b** Difference between NCt and FCt. Only differences significant at the 95% level according to a Hotelling t^2 test (for the fluxes) and a t test (for the divergence) are represented. The Hotelling t^2 test is the multivariate generalization of the t test. The box represents the limits of the nudging domain. **c** Biases of FCt against ERA40. Significance tested and represented as for (b). RMS statistics computed respectively on the divergence, zonal and meridional components of the moisture fluxes in the free domain are labeled on the figure. **d** As (c) but for NCt



(WAMI, Fontaine et al. 1995, consisting in the difference between the 850 and 200 hPa zonal wind averaged over the domain 3°N 13°N , 20°W 20°E), an AEJ index as defined as in Garric et al. (2002) and a regional Sudan and Sahel rainfall index. Though the interannual variability of the latter is not dramatically improved ($r = 0.51$ for the nudged experiment, versus 0.41 for the control), the WAMI fluctuations are better captured with the nudged experiment ($r = 0.66$, versus 0.42 for the free experiment). Our aim here is to pursue their results and analyze more in detail the impact of the nudging on atmospheric dynamics and precipitation interannual variability over West Africa.

Figure 4a, b show the interannual variability of rainfall and moisture divergence over West Africa during the monsoon. The metrics used to quantify the regional year-to-year fluctuations of the WAM is the standard deviation because it does not require in-phase co-variability between the simulations and the observations. The timing of interannual fluctuations will be addressed through linear correlations in Fig. 5.

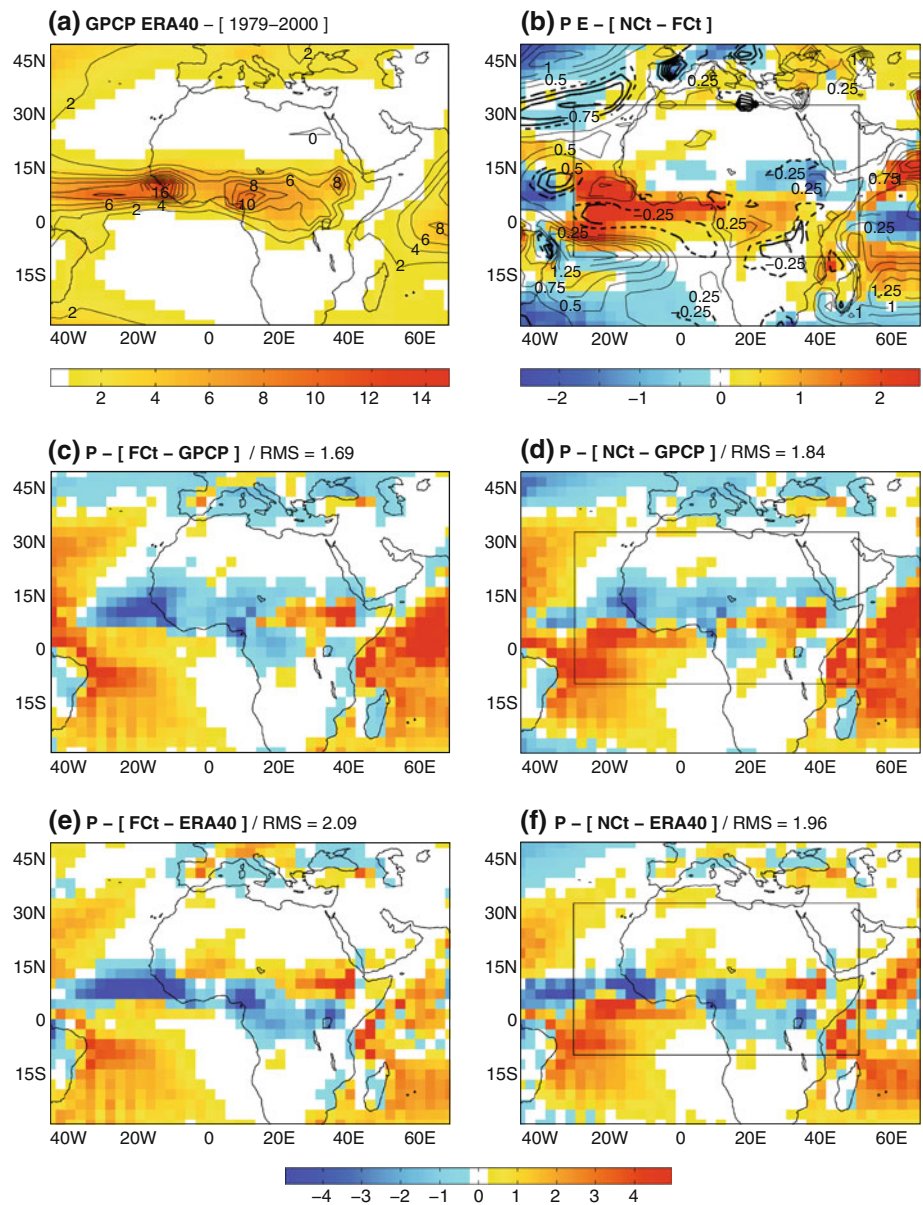
The largest standard deviation values (Fig. 4) are reached at the latitude of the ITCZ, corresponding to the maximum rainfall and moisture convergence (Figs. 2a, 3a). FCt simulates too large interannual variability over Central and East Africa, especially over the wetly biased East African Highlands (Fig. 3c, d). Rainfall interannual variability is generally too low over West Africa (Fig. 4c), as

well as the Eastern Sahara and Mediterranean, and the Atlantic coast off Morocco/Mauritania and Namibia. Rainfall amounts are nonetheless very weak over the latter regions. On the contrary, interannual variability is too high over the southern tropical Atlantic. Roughly similar patterns are found for moisture divergence, but the areas of too low variability are more widespread over Southern Africa and from the Eastern Sahara to northern Arabia.

NCt succeeds at improving the spatial structures and the regional amplitude of interannual variability in moisture divergence (Fig. 4f–h). Results are particularly obvious over the Eastern Sahara, Saudi Arabia and the Eastern Sahel. They are more limited over the Atlantic basin and in the seasonal rainfall amounts (Fig. 4e–g). Hence it is suggested that the grid-point nudging improves the atmospheric dynamics associated to the WAM, corroborating the results of B10 based on regional rainfall indices and dynamical descriptors of the monsoon.

Figure 5 documents the co-variability between observed/reanalyzed and simulated rainfall and moisture divergence, including their year-to-year phasing. FCt only succeeds at simulating observed interannual variability over the tropical oceans (from the western Atlantic basin to the Guinean coast and over the western Indian Ocean) where the prescribed SST forcing has a local impact on deep convection. Correlations between simulated rainfall and GPCP (Fig. 5a) tend to be stronger than for moisture divergence (Fig. 5b).

Fig. 3 **a** JJAS mean rainfall field (mm day^{-1}) according to GPCP (*shading*) and ERA40 (contour), period 1979–2000. See legend for colour shading. Contour interval is 2 mm day^{-1} . **b** Difference in seasonal mean rainfall (*shading*, mm day^{-1}) and evapo-transpiration (contour, mm day^{-1}) between Nct and Fct, period 1979–2000. The *box* represents the limits of the nudging domain. Contour interval is 0.25 mm day^{-1} and the zero contour is omitted. All differences that are not statistically significant at the 95% level according to a *t* test are shaded white or are not contoured. **c** Precipitation biases of Fct (mm day^{-1}) against GPCP. Significance tested and represented as for (b). An RMS statistics computed over the free domain is labeled on the figure. **d** As (c) but for Nct. **e, f** As (c–d) but against ERA40 precipitation



Nct (Fig. 5c, d) logically presents high correlation values within the nudged domain. Correlations with rainfall are nevertheless not always statistically significant, indicating that a realistic large-scale atmospheric dynamics is not a sufficient condition to obtain realistic rainfall. Within the free domain, and particularly over tropical Africa, correlations with rainfall tend however to be stronger than those for moisture divergence. This is remarkably true at the latitude of the Sahel, where rainfall interannual variability is strongly improved (Fig. 5e).

Prescribing realistic lateral conditions makes thus it possible to obtain, to some extent, significant co-variability with observations within the free domain, even if the model climatology strongly resists to the nudging protocol. The part of common variance with the observations is thought

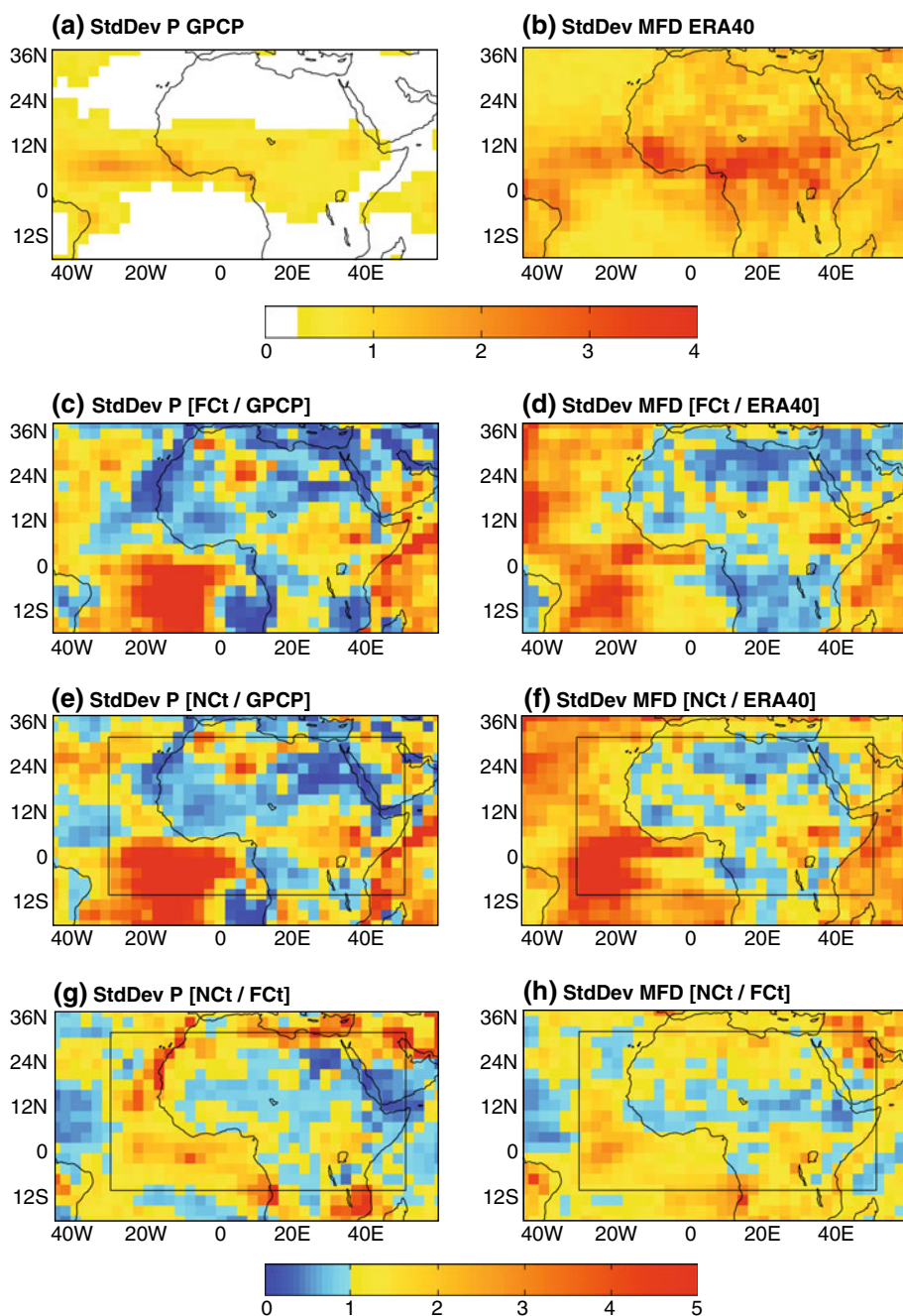
to be a function of the free domain size, a topic widely explored within the regional modeling community (e.g. Jones et al. 1995; Seth and Giorgi 1998; Leduc and Laprise 2008). This issue will not be addressed in the present study, but preliminary tests to the domain size and location suggest that our results are not very sensitive to the prescribed boundaries of the nudging domain.

4 1994 sensitivity studies

4.1 Simulation of 1994 anomalies

The results obtained in Sect. 3.2 remain qualitative and a robust assessment of the nudging impact on the monsoon

Fig. 4 **a** Interannual standard deviation of GPCP seasonal mean rainfall amounts (mm day^{-1}), period 1979–2000. **b** As (a) but for ERA40 seasonal mean moisture flux divergence (mm day^{-1}). **c** Ratio between the standard deviation of FCt rainfall and GPCP. **d** Ratio between the standard deviation of FCt moisture divergence and ERA40. **e, f** As (c, d) but for Nct. **g, h** As (c, d) but ratio between Nct and FCt



predictability would require large ensembles of seasonal integrations. In the present study, we prefer to focus on a specific rainy season that shows large departures from the seasonal climatology. The retained case study is summer 1994, the wettest rainy season of the 1971–2000 period in the Sahel and a neutral year in terms of ENSO activity (Fig. 6a).

F94 is a 30-member control experiment driven by observed 1994 SST (Table 1). N94 is its nudged counterpart. 1994 seasonal SST anomalies are shown on Fig. 6b: they basically consist of warm anomalies over the

Mediterranean (+1K), cold ones in the Gulf of Guinea (-0.7 K) and more generally in the Atlantic (except in the north-western part of the basin) and rather weak warm anomalies in the central Pacific (+0.6 K).

Figure 7 presents the 1994 seasonal anomalies in moisture flux divergence and rainfall, in the reference datasets (GPCP and ERA40) and free and nudged experiments (F94 minus FCt and N94 minus Nct). Moisture flux and divergence anomalies (Fig. 7a) mostly consist of westerly anomalies in the northern low latitudes over West Africa, together with weaker cyclonic anomalies over the

Fig. 5 **a** Interannual correlations between FCt and GPCP seasonal mean rainfall amount in each grid point, period 1979–2000. Correlations that are not significant at the 95% level are shaded white. **b** Correlations between FCt and ERA40 seasonal mean moisture divergence. Significance tested and represented as for (a). **c, d** As (a, b) but for NCt. **e, f** Difference between the correlation fields calculated for NCt and FCt. All differences are shown without significance tests, note the distinct color scale

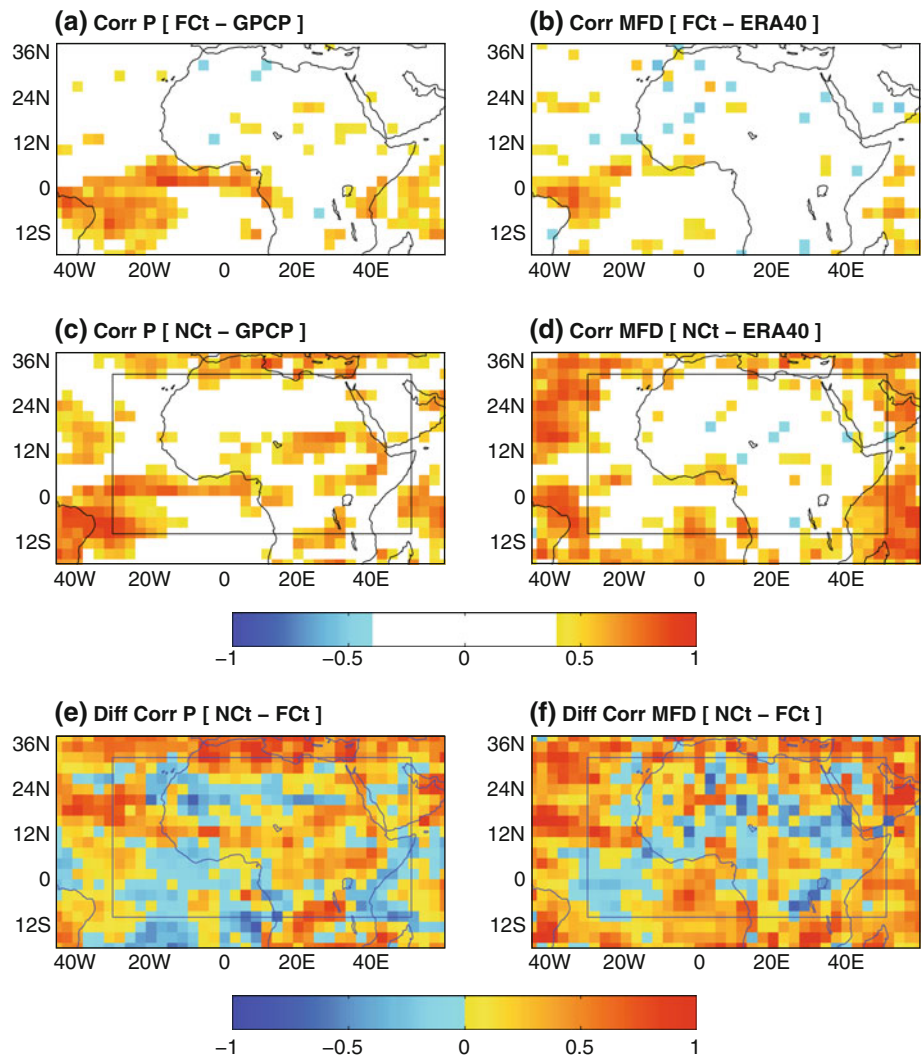
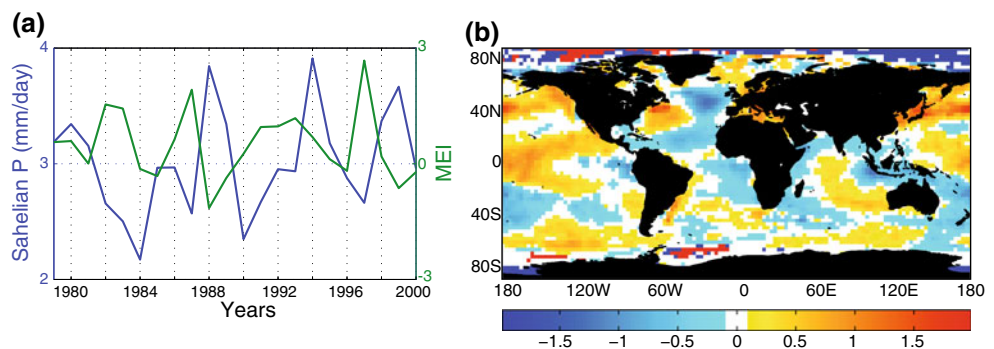


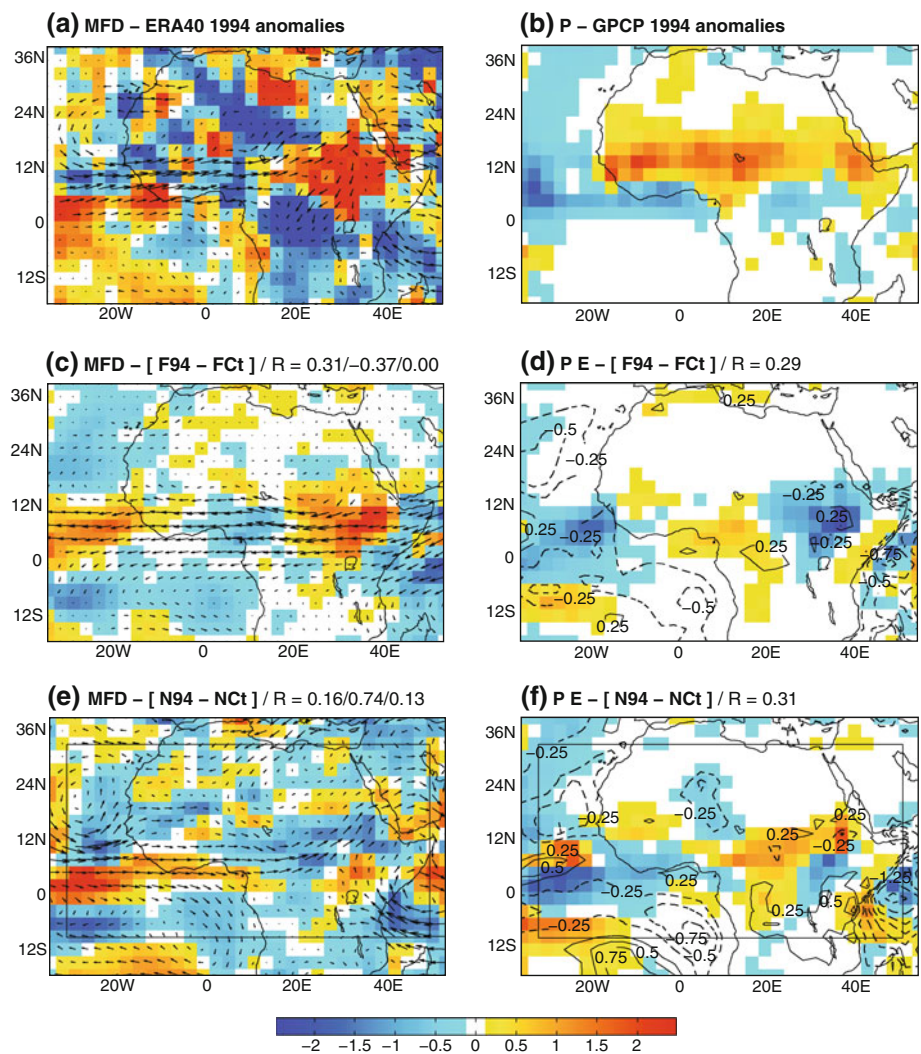
Fig. 6 **a** Blue curve Sahelian (10°N 20°N 20°W 20°E) seasonal mean rainfall (mm day⁻¹), 1979–2000. Green curve seasonal mean Multivariate ENSO index (Wolter and Timlin 1993). **b** SST seasonal mean anomalies in JJAS 1994 with respect to the 1979–2000 climatology. Anomalies that are not statistically significant at the 95% are shaded white



Atlantic Ocean at both northern and southern tropical latitudes. There are also moisture convergence (divergence) anomalies over the western (eastern) Sahel. GPCP data (Fig. 7b) show clear and zonal wet anomalies over the Sahel, continuously from Senegal to Ethiopia. Dry anomalies prevail south of the Sahel, denoting an abnormally northern location of the monsoon front.

When driven by the 1994 SST field (Fig. 6b), Arpege-Climat succeeds at simulating wet conditions over West Africa (Fig. 7d). The amplitude is however largely underestimated, largest departures being located over Central Africa instead of the Sahel, where contrasted wet and dry anomalies are found from West to East. Moreover, the model simulates unrealistic moisture fluxes (Fig. 7b).

Fig. 7 **a** ERA40 vertically integrated moisture flux (*vectors*) and divergence (*shadings*) anomalies in JJAS 1994 with respect to the 1979–2000 climatology. Anomalies that are not significant at the 95% level are shaded white. **b** GPCP seasonal mean rainfall anomalies in JJAS 1994 with respect to the 1979–2000 climatology. Significance tested and represented as for Fig. 2. **c, d** As (**a**) but for the differences between F94-FcT. Contours in (**d**) correspond to surface evapo-transpiration, with a contour interval of 0.25 mm day^{-1} and the zero contour omitted. **e, f** As (**c, d**) but for N94-NCt



Seasonal anomalies in the zonal moisture fluxes over tropical Africa are indeed opposite to ERA40 (i.e. easterly in the model and westerly in the reanalyses). In spite of this sign error, moisture divergence (convergence) anomalies are found over the eastern (western) Sahel, consistently with the reanalyses, and explaining the rainfall anomaly pattern observed on Fig. 7d.

One of the main improvements due to the nudging is the correction of the sign error in the zonal moisture fluxes over Africa (Fig. 7e). The two cyclonic anomaly cells found over the subtropical Atlantic at the limit of the free domain are also better simulated. Moisture divergence is also improved, with in particular convergence anomalies over the central Sahel, but GPCP rainfall anomalies are however still poorly captured (Fig. 7f). Though wet conditions tend to be more prevalent than in F94 (notably over the central Sahel), they remain too limited spatially over West Africa. Even if the monsoon flow seems to penetrate

further north, unrealistic dry anomalies are simulated in Niger and southern Algeria. In spite of higher co-variability with the observations over the 1971–2000 period (Sect. 3.2), the grid-point nudging does not lead to an improved simulation of the heavy rainfall over the Sahel in summer 1994. Consequently, the model biases shown in Figs. 2 and 3 are enhanced in 1994 (not shown). The dry biases over West Africa are locally 100% larger and the zonal dipole between Western Sahel and East Africa still prevails. Moisture divergence is too pronounced over Central and Western Sahel because of the too weak penetration of moisture fluxes from the Atlantic and the Mediterranean. The 1994 rainy season is thus representative of the systematic errors of the model on the control period 1971–2000, except that the amplitude of the biases tends to be larger. This makes 1994 an appropriate season to explore whether a slightly modified nudging protocol could contribute to reduce more efficiently the model biases.

4.2 Sensitivity to nudging strength and ERA filtering

The lack of sensitivity of the model mean state to a quasi-global nudging could result from an inadequate nudging strength. The reference fields towards which the model is relaxed (ERA40 in the present case) could also introduce some numerical artifacts if their solution is too different from the model's basic state. In particular, their high-frequency variability could induce edge effects in the buffer zone between the nudged and the free domain. This would be the case if the simulated high-frequency variability has different spatial/spectral properties. Besides the model's atmospheric physical package (particularly the parameterization of deep convection) that will not be addressed in the present study, another hypothesis involves unrealistic soil moisture boundary conditions and associated precipitation feedbacks (Koster and The GLACE team 2004). It is here proposed to explore these possibilities through sensitivity studies to the nudging strength, the low-pass filtering of the ERA40 nudging fields, the nudging fields themselves (by considering ERA-Interim as an alternative reference

solution), and the effects of total soil moisture boundary conditions.

To that end, the following experiments were designed:

- n94, with a nudging strength divided by 10 compared to N94,
- NA94 and nA94, nudged towards 9-day low-pass filtered ERA40 fields, with a strong (weak) nudging, respectively,
- NB94 and nB94, similarly nudged towards 25-day lowpass filtered ERA40 data.

All integrations are 30-member ensemble seasonal simulations using the same initial conditions as in NCT and N94. I94 (nudged towards ERA-Interim) and experiments conducted with perturbed soil moisture boundary conditions will be discussed in Sects. 4.3 and 4.4 respectively.

Figures 8 and 9 present the effects of the nudging strength (differences between “N” and “n” experiments) and the lowpass filtering of the nudging fields (“N—NA” and “N—NB” differences) on seasonal mean MFD (Fig. 8) and rainfall (Fig. 9). The biases of N94 against

Fig. 8 **a** Biases of N94 moisture fluxes and divergence against ERA40 in JJAS 1994. Significance tested and represented as for Fig. 2.
b As (a) but for the differences between N94 and n94.
c As (a) but for the differences between N94 and NA94.
d As (a) but for the differences between NA94 and nA94.
e As (a) but for the differences between N94 and NB94.
f As (a) but for the differences between NB94 and nB94

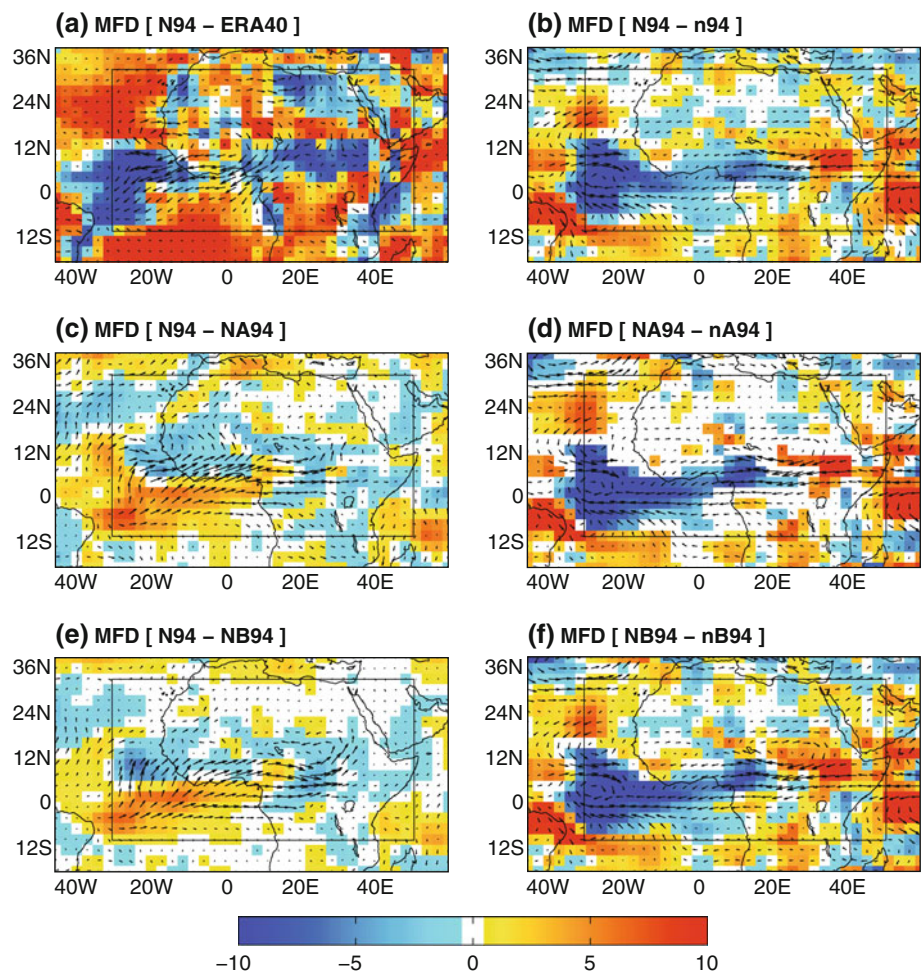
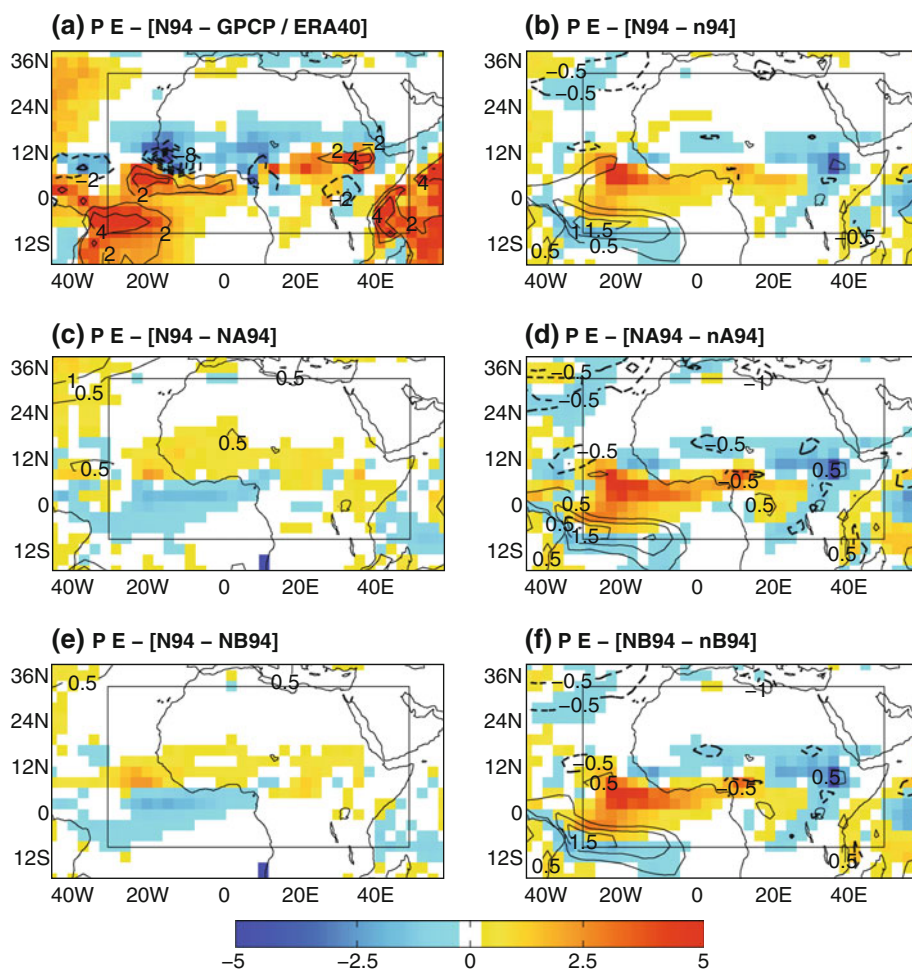


Fig. 9 As Fig. 8 but for rainfall (shadings) and surface evapotranspiration (contours). Significance tested and represented as for Fig. 2. Contour interval is 0.5 mm day^{-1} and the zero contour is omitted



GPCP/ERA40 are shown in Figs. 9a and 10a, confirming their resemblance with the average errors of the model (Figs. 2, 3).

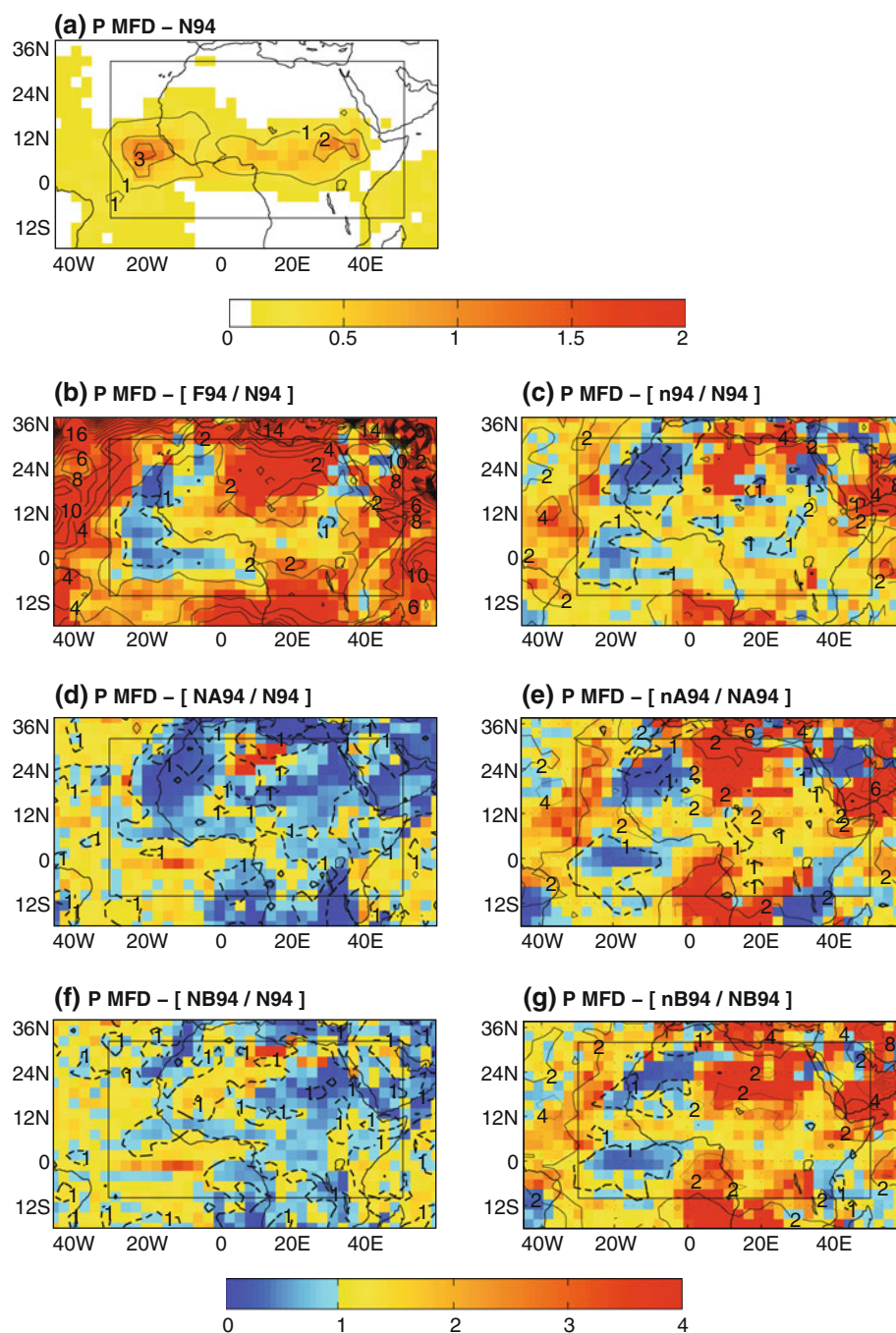
Filtering the nudging fields does not drastically modify the model mean climate over West Africa. Rainfall tends indeed to be slightly less abundant in NA94 and NB94 experiments (Fig. 9c–e) due to less penetrating moisture fluxes originating from the Atlantic basin (Fig. 8c–e), which contributes to reduce moisture flux convergence over the Sahel. The amplitude of such differences is rather weak compared to that of the model systematic errors (Figs. 8a, 9a). Possible causes for such differences concern a modified intraseasonal activity, a topic that will be investigated in a companion paper. As far as seasonal mean climate is concerned, it seems therefore that the high-frequency component of the ERA40 nudging fields is not at the origin of the model’s persisting biases.

The relaxation strength appears also to be weakly involved. Whatever filtering is applied to ERA40 fields, a weaker nudging favors slightly higher rainfall amounts over localized parts of the Sahel (Fig. 9b–f) in relationship with stronger easterly component of the moisture

fluxes over equatorial and tropical Africa (Fig. 8b–f). The too weak monsoon flow and moisture advection from the Mediterranean are not enhanced when relaxation strength is divided by 10. Once again the model systematic errors are not much changed. For this reason, we conclude that the design of our nudging experiments is not the reason for the limited impact on model climatology.

In order to evaluate the consequences of the nudging protocol on the skill of the model in reproducing the 1994 seasonal mean rainfall and MFD fields, Fig. 10 shows the inter-member spread (i.e. the model internal variability) in rainfall and moisture flux divergence for the JJAS 1994 rainy season. Largest values of spread for N94 (Fig. 10a) are logically found at the latitude of the maximum rainfall/moisture convergence. Two localized pockets of large spread, located over the close northern Atlantic and tropical East Africa, are well individualized. Though not completely null, the spread in the nudged domain is greatly reduced. This is particularly true for MFD, because both horizontal wind and specific humidity are nudged variables (Sect. 2).

Fig. 10 **a** Inter-member spread, estimated by the standard deviation computed on seasonal mean fields, in Ct94 rainfall (*shadings*) and MFD (contours). Contour interval is 1 mm day^{-1} . **b** Ratio between the inter-member spread of F94 and N94. **c** As (**b**) but between n94 and N94. **d** As (**b**) but between NA94 and N94. **e** As (**b**) but between nA94 and NA94. **f** As (**b**) but between NB94 and N94. **g** As (**b**) but between nB94 and NB94



F94 displays larger spread values than N94 (Fig. 10b), especially within its nudged domain but also over parts of West Africa (the Eastern Sahara, the south of the Congo basin and East Africa). Surprisingly, internal variability in rainfall amounts (and to a lesser extent in MFD) is lower in F94 along the Atlantic coast of West Africa. Artificial edge effects along the westerly bound of the nudging mask could be involved. This is however unlikely, since sensitivity experiments to the domain size revealed that our conclusions are verified even if the western bound of the nudging mask is shifted westwards (not shown).

Nudging towards lowpass filtered ERA40 fields largely decreases internal variability over the free domain (Fig. 10d–f), suggesting that the high-frequency variability in the lateral boundary conditions contribute to generate inter-member spread. A weaker relaxation (Fig. 10c–g) tend to increase (reduce) the spread along the northerly and southerly (westerly) bounds of the nudging domain, which corresponds more or less to the pattern already obtained for F94. The model tends thus to converge towards its own solution. Such results also suggest that potential edge effects due to the nudging protocol could predominantly

concentrate along the easterly/westerly bounds, indicative of possible inconsistencies associated with the large-scale zonal fluxes over the domain (e.g. the AEJ or TEJ). This could be attributed to inappropriate nudging fields. Section 4.3 investigates the influence of the prescribed lateral boundary conditions, by analyzing integrations nudged towards newly released ERA-Interim reanalysis.

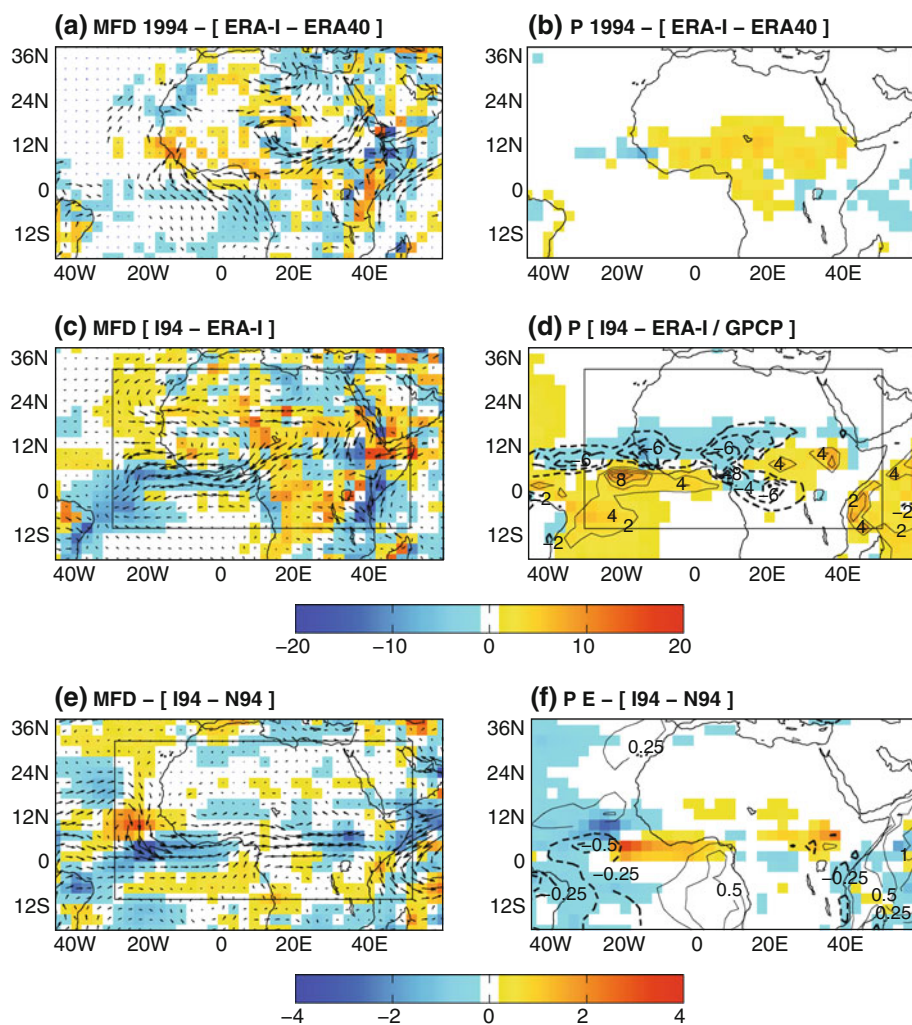
4.3 ERA40 versus ERA-Interim

The differences between ERA40 and ERA-Interim in terms of rainfall and MFD are shown in Fig. 11a, b for the JJAS 1994 rainy season. Over Central and West Africa rainfall amounts are significantly larger in ERA-Interim and more consistent with GPCP (Fig. 11b), especially at the latitude of the Sahel. Vertically integrated moisture fluxes and divergence show weaker differences between the two datasets, with in particular no clear enhancement of the fluxes originating from the tropical Atlantic. Northerly fluxes from the Eastern Mediterranean are even weaker in

ERA-Interim. As a result, moisture flux divergence over the Sahel is not dramatically modified, at least for the 1994 rainy season. This is consistent with the water budget analysis recently conducted by Meynadier et al. (2010b) that suggests that the lack of convergence over the Sahel combined with the presence of a deep layer of northerly dry air advected at mid-levels might block the development of deep convection in the ECMWF model and hence the northward propagation of the monsoon.

Biases of I94 experiment against ERA-Interim (Fig. 11c, d) are qualitatively similar to those of N94 against ERA40 (Figs. 8, 9). Simulated rainfall is still located too close to the Guinean coast (Figs. 11d, 9a). Moisture divergence (Figs. 11c, 8a) remains similarly too large over the Sahel and too weak over East Africa. As far as West Africa is concerned, unrealistic MFD values result in both N94 and I94 experiments of too weak penetration of the moisture fluxes from the Atlantic. As a consequence, the differences between N94 and I94 (Fig. 11e, f) are very weak compared to the amplitude of the model's biases over

Fig. 11 **a** Vertically integrated moisture flux (*vectors*) and divergence (*shadings*) differences between ERA40 and ERA-Interim, JJAS 1994. **b** Rainfall differences (mm day^{-1}) between ERA40 and ERA-Interim, JJAS 1994. **c** Vertically integrated moisture flux (*vectors*) and divergence (*shadings*) biases of I94 against ERA-Interim. **d** Rainfall biases of I94 against GPCP (*shadings*) and ERA-Interim (*contours*). Contour interval is 0.25 mm day^{-1} with the zero contour omitted. **e** Vertically integrated moisture flux (*vectors*) and divergence (*shadings*) differences between I94 and N94. **f** Rainfall (*shadings*) and surface evapotranspiration (*contours*) differences between I94 and N94. For all panels, significance is tested and represented as for Fig. 2



the region. Rainfall amounts are locally larger over the Central Sahel in I94, due to decreased MFD and stronger incoming moisture fluxes penetrating over West Africa from the Atlantic Ocean.

Though I94 tends to show slightly better results than N94, the largest part of the biases remains unchanged. The reference fields towards which the model is relaxed do not seem therefore to be involved in the persisting biases noted in previous sections. This leads us to explore our last hypothesis, involving land surface boundary conditions.

4.4 Sensitivity to soil moisture

In order to explore to what extent the model dry biases over West Africa could relate to unrealistic land surface conditions or be amplified through a positive soil moisture-precipitation feedback, the ISBA land surface component of the Arpege-Climat model was nudged towards the second Global Soil Wetness Project (GSWP-2; Dirmeyer et al. 2002) monthly climatology (Decharme and Douville 2006). This series of additional experiments (Table 1) enable us to discuss the sensitivity of the WAM to soil moisture in the Arpege-Climat atmospheric general circulation model (AGCM). This is of interest because the feedback between soil moisture and rainfall appears to be uncertain (Koster and The GLACE team 2004; Douville et al. 2007; Moufouma-Okia and Rowell 2010) and model dependent. Hence, we propose here to suppress the continent-ocean coupling and prescribe realistic soil moisture conditions.

GSWP-2, launched by the global energy and water cycle experiment (GEWEX) to provide high-resolution global soil moisture climatologies, is an off-line integration of 12 LSM, driven by NCEP-DOE AMIP-II reanalyses and GPCP rain-gauge data on the 1986–1995 period. We use here the moisture fields calculated by the ISBA model of CNRM. Such an off-line integration is thought to provide more reliable estimates of the observed soil wetness than on-line integrations, and thus to correct part of the biases in soil moisture. It is also perfectly consistent with the Arpege-Climat model, which avoids the difficult issue of vertical interpolation of soil wetness profiles. Finally, it is hopefully more reliable than the ERA40 or ERA-Interim soil moisture climatology, which is still based on a relatively crude data assimilation technique. Note that only deep soil moisture is nudged towards the GSWP-2 monthly mean climatology so that surface soil moisture is still interactive even if its variability is damped by the nudging. More details about the relaxation technique can be found in Douville et al. (2007). Three soil moisture sensitivity experiments were conducted: a control experiment, FS94, driven by observed 1994 monthly mean SST, NS94 and

IS94 which are additionally nudged towards the ERA40 and ERA-Interim atmospheric reanalyses respectively.

Figure 12 presents the temporal and spatial aspects of the perturbation introduced by the soil nudging in 1994. At the end of the rainy season, after the refill of the water reserves, the total water content reaches between 50 and 120 kg m⁻² in the free experiments, depending on the member. One can note that the spread is larger for F94 experiment than for N94 or I94, and that the curves of the different members are approximately parallel in both nudged experiments. In other words, the differences between the members tend to be constant over the season, and remain almost equal to those induced by the initial conditions. This is not the case for F94. This result suggests that the seasonal rainfall amount and the distribution of rain spells within the season are strongly controlled by the nudging, i.e. by large-scale conditions around West Africa. Focus will be given on the intraseasonal timescale in the second part of this study.

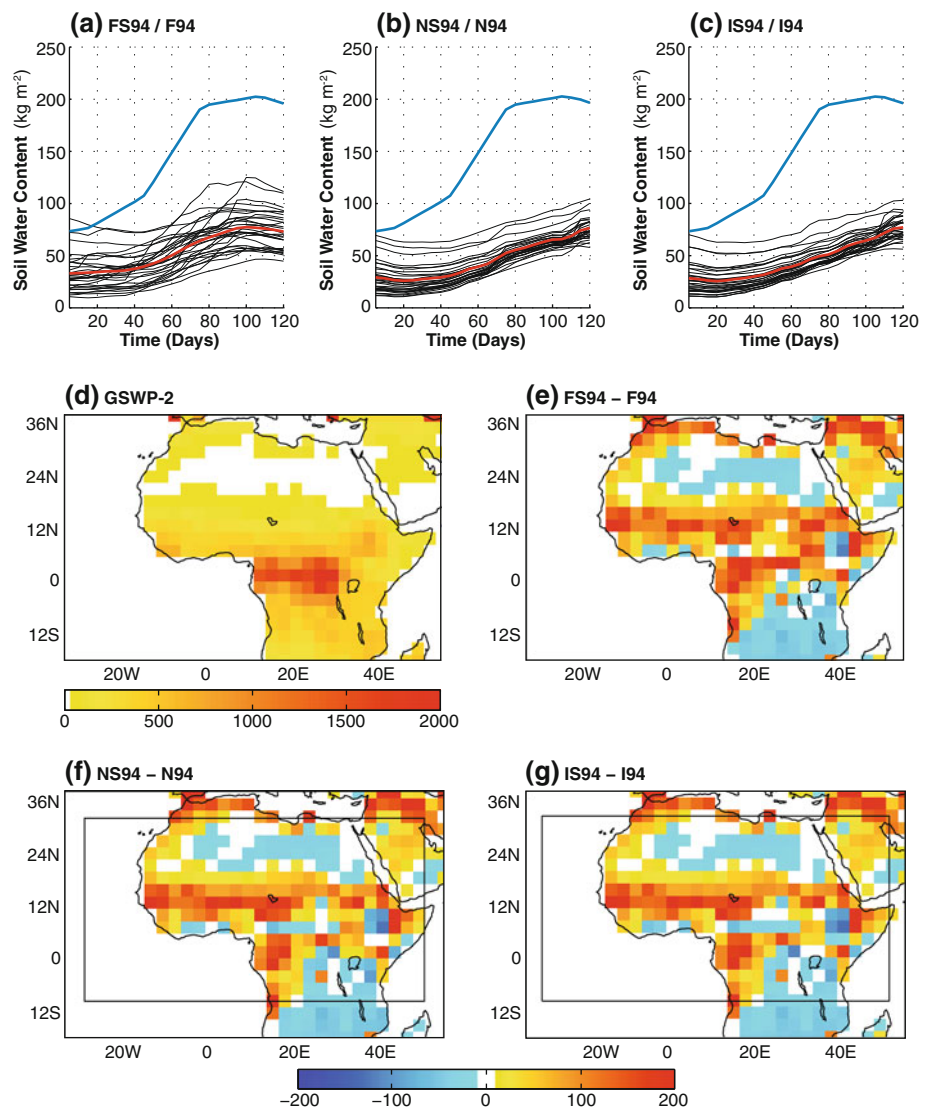
In the experiments including soil moisture nudging, the total soil water content reaches 200 kg m⁻² in late September, i.e. almost three times the value obtained with an interactive LSM. The spread between the different members is also completely suppressed. Spatially, the Sahel and the Congo basin are the most concerned regions. GSWP-2 leads to add up to 200 kg m⁻² in localized areas (such as Senegal or the surroundings of Lake Chad) but provides less soil wetness in the central Sahara and Southern Africa.

Figure 13 shows the effects of the soil moisture perturbation on moisture flux divergence and rainfall over West Africa. In order to quantify to what extent the model systematic biases (Figs. 2, 3) are reduced or enhanced, correlation coefficients between these differences and the biases of the corresponding experiment are labeled on the figure (e.g. the spatial correlation between the bias of F94, defined as F94 minus the reference field [ERA40 or GPCP], and the difference FS94 minus F94). The correlations are computed on all grid points included in the free domain.

The most dramatic effect of the soil nudging logically concerns surface evapo-transpiration E . The correspondence between Figs. 12e–g and 13a–e is quite obvious, and E is greatly enhanced over the overall Sahel and more locally over the Congo basin (and reduced over Southern Africa). Near Lake Chad, the difference with soil-free experiments reaches +1 mm day⁻¹.

Consequences on precipitation are more diffuse. The negative correlations with the spatial pattern of the model biases indicate that the latter tend to be reduced in the soil nudging experiments. The amplitude of the improvement is nevertheless between two and three times lesser than that of the biases (Fig. 3). Rainfall amounts are generally larger in West Africa, and the area showing significant

Fig. 12 **a** Total soil water content (kg m^{-2}) in FS94 (cyan) and F94 (black) over the Sahel (10°N – 20°N , 20°W – 20°E), JJAS 1994. The red curve corresponds to the ensemble mean in F94. **b** As (a) but for NS94 and N94. **c** As (a) but for IS94 and I94. **d** Seasonal mean soil water content according to GSWP-2, JJAS 1994. **e** Difference (kg m^{-2}) between the seasonal mean soil water content in FS94 and F94. Differences that are not significant at the 95% level are shaded white. **f** As (e) but for NS94 and N94. **g** As (e) but for IS94 and I94



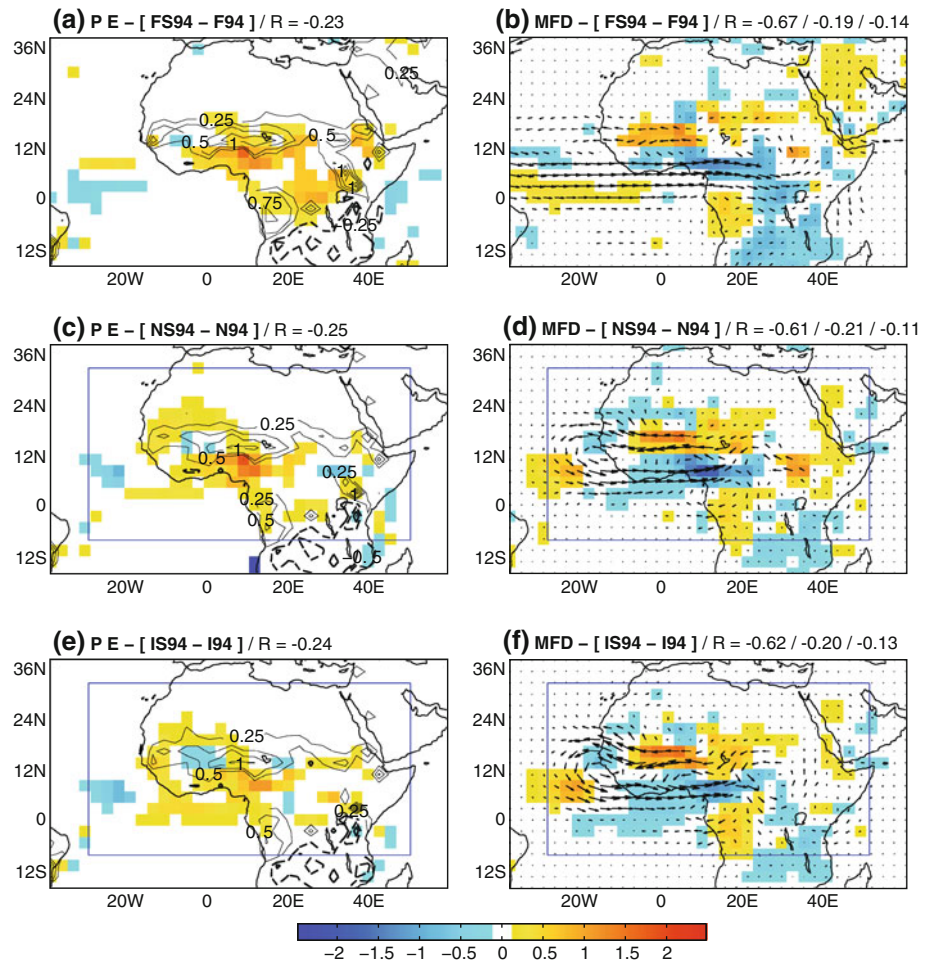
differences extends continuously from Western Sahara to Central Africa. This confirms that the feedback between soil moisture and rainfall is generally positive (Douville et al. 2001; Koster and The GLACE team 2004; Douville et al. 2007). Sensitivity to soil wetness is roughly similar for the runs conducted with or without atmospheric nudging, which validates such sensitivity experiments performed on Regional Climate Models, since the response of the regional atmosphere to the surface perturbation is not modified by the prescribed lateral conditions.

Over West Africa, the strongest response of rainfall is shifted southwards compared to that of evapo-transpiration, especially over the central and western Sahel. At least two mechanisms could explain this shift: (1) enhancing soil moisture and surface evaporation cools the lower troposphere, resulting in weaker inter-hemispheric energy gradients and in a weaker monsoon flow; (2) GSWP-2 soil moisture boundary conditions increase surface evaporation

north of the simulated inter-tropical convergence zone, which enhances rainfall south of the Sahel through a moistening of the southward Harmattan flux. To verify these hypotheses we calculated the vertically integrated moist static energy (MSE) between the surface and 850 hPa (not shown), where $\text{MSE} = gZ + \text{CpT} + \text{LQ}$, with MSE in kJ kg^{-1} , gZ is potential energy, CpT sensible energy and LQ latent energy. We also analyzed the different components of MSE, such as described above. The results revealed that air surface (i.e. CpT) is indeed decreased by enhanced surface evaporation. However, LQ is more significantly increased due to larger water content in the air mass. Consequently, inter-hemispheric MSE gradients are slightly enhanced in NS experiments (not shown). Hypothesis (1) is thus rejected.

The analysis of vertically integrated moisture fluxes (Fig. 13b–f) makes it possible to validate hypothesis (2). In GSWP-2 driven integrations, easterly (westerly) moisture

Fig. 13 **a** *Shadings* difference in seasonal mean rainfall (mm day^{-1}) between FS94 and F94. *Contours* difference in seasonal mean evapotranspiration (mm day^{-1}). Contours interval is 0.25 mm day^{-1} , and the zero contour is omitted. **b** *Vectors* difference in the seasonal mean integrated moisture fluxes between the same experiments. *Shading* difference in seasonal mean moisture divergence (mm day^{-1}). For all panels, significance is tested and shown as for Fig. 2. **c, d** As **(a, b)** but for NS94 and N94. **e, f** As **(a, b)** but for IS94 and I94



fluxes are favored at the latitude of the Sahel (the Guinean coast), which corrects the model biases ($r \approx -0.65$) but generates enhanced divergence (convergence) at the latitude of the Sahel (Guinea). There is good correspondence between rainfall and moisture convergence. This explains why rainfall maxima are still shifted southwards compared to observations, even in experiments driven by GSWP-2 soil moisture.

To sum up, using GSWP-2 soil moisture boundary conditions limits the dry biases over West Africa, but moisture convergence and rainfall maximum are still placed too close to the Guinean coast and the land surface hydrology is not the key explanation for the Arpege-Climat systematic errors over the Sahel.

5 Conclusions

In this work we used the so-called grid point nudging technique (Bielli et al. 2010; Douville 2009; Jung et al. 2009) to guide the CNRM AGCM Arpege-Climat towards ERA40 reanalyses at the near-global scale outside West

Africa (10°S – 32°N , 30°W – 50°E). This methodology enables us (1) to document the origin of the regional biases of the model, (2) to disentangle regional versus large-scale sources of WAM interannual variability, (3) to conduct sensitivity experiments to lateral or surface boundary conditions.

Results show that the WAM model climatology is barely modified by a quasi-global nudging. Unrealistic longitudinal gradients between too dry (wet) conditions in West (East) Africa in Arpege-Climat still prevail in nudged experiments. Southerly (northerly) moisture fluxes originating from the tropical Atlantic (eastern Mediterranean) are too weak, inducing too low moisture convergence over the Sahel. The location and modulus of the basic features of the WAM dynamics (the African and Tropical Easterly Jets and the lower-layer monsoon flow) are not dramatically improved by realistic lateral boundary conditions. Maximum rainfall and convergence are also located too close to the Guinean coast. These statements are true in both free and nudged experiments, confirming those of Bielli et al. (2010). They are verified for the 1971–2000 period and are enhanced during the abnormally wet 1994 rainy season.

The persistence of such biases in the relaxed atmospheric simulations could be attributed to (1) an inappropriate nudging protocol, including possible numerical artifacts caused by the nudging strength or the chaotic high-frequency variability of the nudging fields; (2) an inadequacy of the nudging fields, i.e. an inconsistency between the model solution and the one provided by the reanalyses; (3) unrealistic land surface boundary conditions; (4) deficiencies in the atmosphere physical parameterizations. In the present study, points (1) to (3) have been explored with emphasis given on the 1994 case study and the use of 30-member ensemble experiments to ensure the robustness of the results.

- (1) Two additional series of experiments were performed, for which the strength of the relaxation was divided by 10, and the nudging fields provided by ERA40 were low-pass filtered. Frequencies above 9 days and 25 days were successively removed. Results show that the dry biases over West Africa are found whatever nudging strength is used, and whatever nudging fields (i.e. unfiltered or low-pass filtered ERA40) are considered. Hence, the experimental design does not seem to qualitatively influence our results and does not modify any of our conclusions.
- (2) Another integration, nudged towards ERA-Interim, documents the sensitivity to the reference nudging fields. ERA-Interim shows larger rainfall amounts over West Africa during the monsoon. Dynamical fields, in 1994, are however close to those provided by ERA40. Nudged integrations towards ERA-Interim do not reveal a stronger reduction of model biases over West Africa compared to the use of ERA40. In other words, modifying the lateral boundary conditions does not imply strong changes in the simulation of the WAM.
- (3) The strength of the land–atmosphere coupling is highly model dependent over West Africa (Koster and The GLACE team 2004) and has been here damped rather than suppressed through the nudging of the ISBA land surface model towards the GSWP-2 monthly climatology. More importantly, the nudging leads to increased and presumably more realistic seasonal mean surface evaporation over the Sahel, and thereby to improved monsoon rainfall over West Africa. While this result confirms the relevance of a positive soil moisture feedback for the simulation of WAM precipitation, the land surface hydrology is however not the main explanation for the model errors.

Further investigations are planned such as and the use of recently released surface albedo satellite data. The influence of the model physical package, including the parameterization of convective processes (point 4), will also

require new integrations that are beyond the scope of the present study.

In addition to the effects of the nudging technique on the model climatology, the WAM interannual variability was also briefly discussed. The results remain qualitative because they depend on a single series of 30-year integrations. Together with those presented in B10, they nonetheless suggest that a quasi-global nudging notably improves the simulated interannual variability of the WAM dynamics. In 1994, however, Arpege-Climat failed at reproducing the amplitude and the spatial extent of the very strong wet anomalies, even when relaxed towards ERA40 or ERA-Interim out of the region.

Several questions arise from these preliminary findings. Does the nudging show a stronger impact on the simulation of intra-seasonal variability, such as the succession of dry and wet spells during the rainy season? Does it lead to a significant control on the day-to-day variability and how the rainfall chronology compares with the observations? Do the different members or the summer 1994 ensemble experiments show similar temporal fluctuations? Such questions will be addressed in Part II.

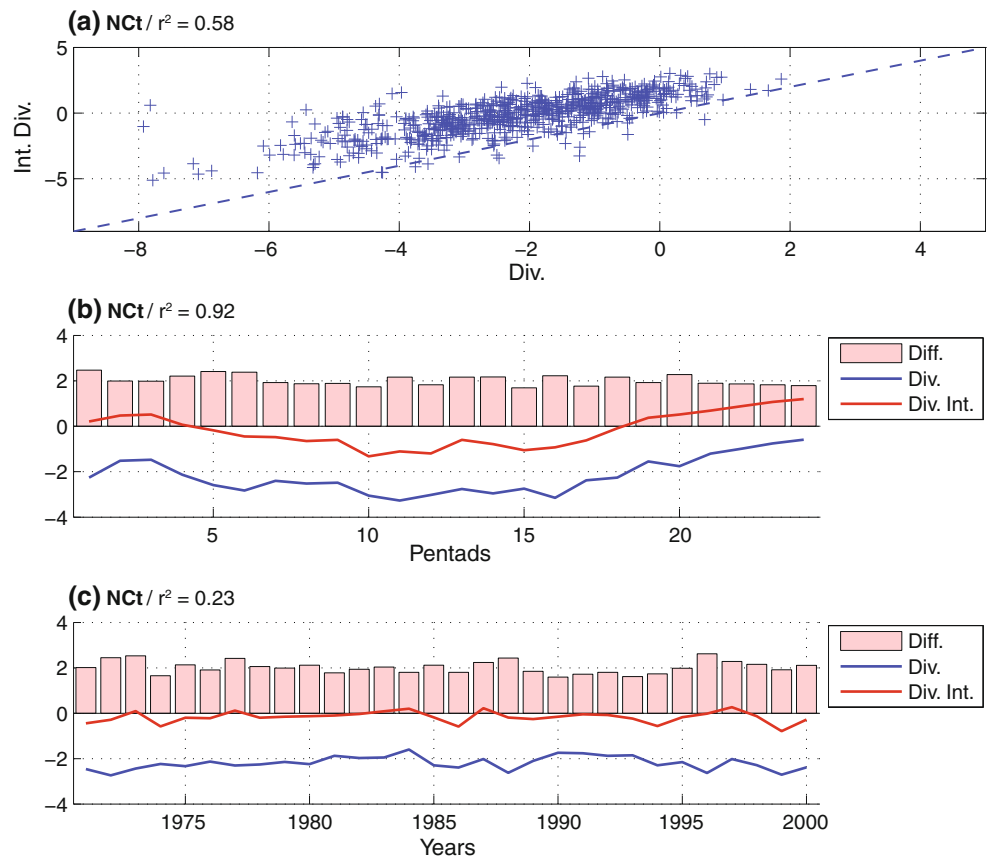
Acknowledgments Based on a French initiative, AMMA was built by an international scientific group and is currently funded by a large number of agencies, especially from France, the United Kingdom, the United States, and Africa. It has been the beneficiary of a major financial contribution from the European Community's Sixth Framework Research Programme. (Detailed information on scientific coordination and funding is available online at the AMMA International Web site at <http://www.amma-international.org>). ERA40 data were downloaded from <http://www.ecmwf.int>. GPCP data were downloaded from <http://www.cdc.noaa.gov>. Thanks are also due to the French ANR IRCAAM project for supporting the development of the nudging technique, and to S. Bielli, F. Chauvin, J-F. Guérémy, F. Guichard, J-P. Lafore, J-L. Redelsperger, R. Roehrig and A. Voldoire for helpful discussions concerning this work. The authors are also very grateful to M. Déqué for his support in using the Arpege-Climat model, and to O. Bock, R. Meynadier and P. Roucou for the computation of the atmospheric water budget.

Appendix: Methodology for the computation of the moisture fluxes

Calculating the atmospheric water budget over a given area is not an easy task because of several methodology problems that can arise at different stages of the computation (Meynadier et al. 2010a):

- (1) reanalyses do not offer the possibility to obtain realistic closure terms for the atmospheric water vapor, because of data assimilation during the integration of numerical weather models.
- (2) tropical rainfall fields in atmospheric models are subject to huge uncertainties because of the perfectible parameterization of deep convective processes.

Fig. 14 a Scatter plot intersecting the pentad mean moisture divergence (mm day^{-1}) over the Sahel (10°N – 20°N , 20°W – 20°E) computed with daily pressure fields (abscissa) and with vertical integrations on the model levels at each model time step (ordinates), JJAS 1971–2000. The common variance between the two series is labeled on the figure.
b Seasonality of moisture divergence according to daily pressure fields (*blue curve*) and 30-min-resolution fields available on sigma levels (*red curve*) for each pentad of the season. *Bars* difference between the two methods of vertical integration (c) As (b) but for seasonal means, period 1971–2000



- (3) daily and even 6-hourly model outputs sub-sample the diurnal cycle, which may lead to wrong representations of, e.g. afternoon tropical storms.
- (4) vertical integration of, e.g. moisture fluxes, are somewhat uncertain because they are often based on a rather low number of pressure levels, interpolated from the model sigma levels.

When working with a GCM, one is still submitted to the errors linked to point (2). It is however possible to estimate to what extent points (3) and (4) may contribute to wrong estimates of the different terms of the equation for water vapor closure. To that end, we computed daily vertically integrated moisture fluxes based on daily outputs interpolated on similar pressure levels as those available for ERA40 reanalyses, and alternatively, moisture fluxes integrated on the model sigma levels at each time step (30 min here). In other words, the first method is that applied on reanalyzed data, but the second one offers better estimates of the moisture fluxes and theoretically allows for a perfect water vapor closure in each grid point. The results are shown in Figs. 14 (for the Sahel) and 15 (over Africa).

Figure 14 shows that, over the Sahel, the two methods lead to a difference of 2 mm day^{-1} . Daily fields overestimate moisture divergence over the Sahel. The error is almost constant from early June to late September

(Fig. 14b) and, to a lesser extent, from 1 year to another (Fig. 14c). For comparison purposes, the difference between ERA40 rainfall and GPCP estimates, shown on Fig. 3 to be rather marked over the region, is 0.5 mm day^{-1} . The methodology for the computation of moisture fluxes is thus of primary importance, and has a first order impact for the water vapor closure term.

Figure 15 shows the JJAS climatological integrated moisture fluxes and divergence for each grid point over Africa, and the error due to the computation method at each grid point. Note that the color scale is the same for the seasonal mean field and the differences between the two computation methods. The model climatology (Fig. 15a) shows the well-known features of large-scale atmospheric circulation over Africa, with inter-tropical moisture convergence located north of the equator and the very strong southerly moisture fluxes related to the Indian monsoon and found over the western Indian Ocean. Errors (Fig. 15b) confirm that moisture divergence is over-estimated over the Sahel when daily pressure fields are used. On the contrary, enhanced moisture convergence takes place over the Guinean belt. Daily pressure fields tend thus to exaggerate the model climatology.

For these reasons, all figures presented in this paper result of moisture fluxes calculated at the model time step

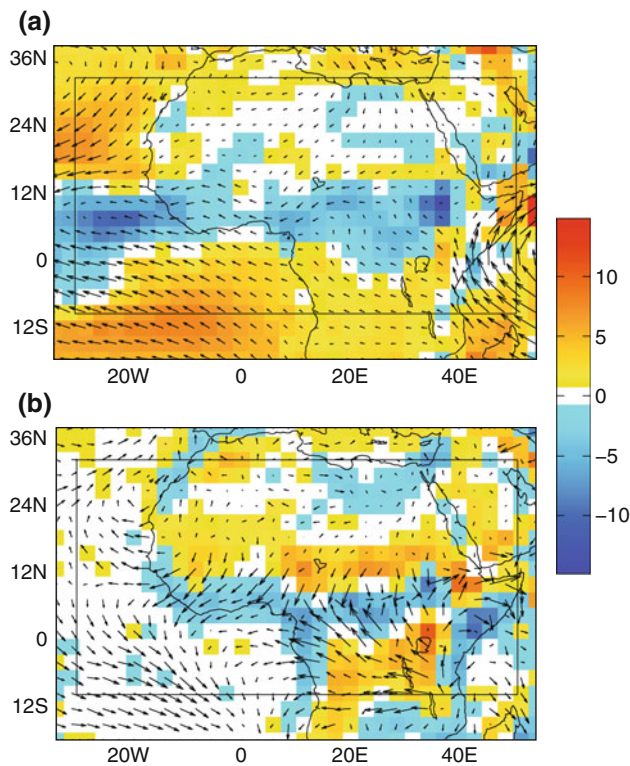


Fig. 15 **a** Seasonal mean moisture fluxes integrated over the air column (*vectors*) and moisture divergence (*shading*), period JJAS 1971–2000. **b** Difference between the two methods of vertical integrations. Significance tested and shown as for Fig. 2

and integrated on sigma levels. Errors nonetheless persist when comparisons with reanalyses are performed, because vertically integrated moisture fluxes are not available for these datasets.

References

- Alexandru A, de Elia R, Laprise R, Separovic L, Biner S (2009) Sensitivity study of regional climate model simulations to large-scale nudging parameters. *Mon Weather Rev* 137:1666–1686
- Biasutti M, Sobel AH, Camargo SJ (2009) The role of the Sahara low in summertime Sahel rainfall variability and change in the CMIP3 models. *J Clim* 22:5755–5771
- Bielli S, Douville H, Pohl B (2010) Understanding the West African monsoon variability and its remote effects: an illustration of the grid point nudging methodology. *Clim Dyn* 35:159–174. doi: [10.1007/s00382-009-0667-8](https://doi.org/10.1007/s00382-009-0667-8)
- Bouali L, Fontaine B, Philippon N, Lémond J (2008) Performance of DEMETER calibration for rainfall forecasting purposes: application to the July–August Sahelian rainfall. *J Geophys Res* 113:1616–1620
- Bougeault P (1985) A simple parameterization of the large-scale effects of cumulus convection. *Mon Weather Rev* 113:2108–2121
- Cook KH, Vizy EK (2006) Coupled model simulations of the West African monsoon system: 20th and 21st century simulations. *J Clim* 19:3681–3703
- Decharme B, Douville H (2006) Uncertainties in the GSWP-2 precipitation forcing and their impacts on regional and global hydrological simulations. *Clim Dyn* 27:695–713
- Dirmeyer PA, Gao X, Oki T (2002) The second global soil wetness project GSWP2: science and implementation plan. IGPO publication series 37, International GEWEX Project Office, pp 65
- Douville H (2009) Stratospheric polar vortex influence on Northern hemisphere winter climate variability. *Geophys Res Lett* 36:L18703. doi: [10.1029/2009GL039334](https://doi.org/10.1029/2009GL039334)
- Douville H, Chauvin F, Broqua H (2001) Influence of soil moisture on the Asian and African monsoons. Part I: mean monsoon and daily precipitation. *J Clim* 14:2381–2403
- Douville H, Salas-Mélia D, Tyteca S (2006) On the tropical origin of uncertainties in the global land precipitation response to global warming. *Clim Dyn* 26:367–385. doi: [10.1007/s00282-005-0088-2](https://doi.org/10.1007/s00282-005-0088-2)
- Douville H, Conil S, Tyteca S, Voltaire A (2007) Soil moisture memory and West African monsoon predictability: artefact or reality? *Clim Dyn* 28:723–742. doi: [10.1007/s00382-006-0207-8](https://doi.org/10.1007/s00382-006-0207-8)
- Fontaine B, Janicot S, Moron V (1995) Rainfall anomaly patterns and wind field signals over West Africa in August (1958–1989). *J Clim* 8:1503–1508
- Garric G, Douville H, Déqué M (2002) Prospects for improved seasonal predictions of monsoon precipitation over Sahel. *Int J Climatol* 22:331–345
- Hourdin F, The AMMA-MIP team (2010) AMMA-model intercomparison project. *Bull Am Meteor Soc* 91:95–104
- Huffman GJ, Adler RF, Rudolf B, Schneider U, Keehn PR (1997) The global precipitation climatology project (GPCP) combined precipitation dataset. *Bull Am Meteorol Soc* 78:5–20
- Joly M, Voltaire A, Douville H, Terray P, Royer J-F (2007) African monsoon teleconnections with tropical SSTs: validation and evolution in a set of IPCC4 simulations. *Clim Dyn* 29:1–20. doi: [10.1007/s00382-006-0215-8](https://doi.org/10.1007/s00382-006-0215-8)
- Jones RG, Murphy JM, Noguer M (1995) Simulation of climate change over Europe using a nested regional-climate model. I: assessment of control climate, including sensitivity to location of lateral boundaries. *Quart J Roy Meteorol Soc* 121:1413–1449
- Jung T, Palmer T, Rodwell M, Serrar S (2009) Understanding the anomalously cold European winter of 2005/06 using relaxation experiments. ECMWF technical memorandum, pp 20
- Koster R, The GLACE team (2004) Regions of strong coupling between soil moisture and precipitation. *Science* 305:1138–1140
- Leduc M, Laprise R (2008) Regional climate model sensitivity to domain size. *Clim Dyn* 32:833–854. doi: [10.1007/s00382-008-0400-z](https://doi.org/10.1007/s00382-008-0400-z)
- Leroux S, Hall NMJ (2009) On the relationship between African easterly waves and the African easterly jet. *J Atm Sci* 66:2303–2316
- Leung LR, Mearns LO, Giorgi F, Wilby RL (2003) Regional climate research - needs and opportunities. *Bull Am Meteor Soc* 84:89–95
- Meynadier R, Bock O, Guichard F, Boone A, Roucou P, Redelsperger JL (2010a) The West African monsoon water cycle. Part I: a hybrid water budget dataset. *J Geophys Res* (in press)
- Meynadier R, Bock O, Gervois S, Guichard F, Redelsperger J-L, Agusti-Panareda A, Beljaars (2010b) The West African monsoon water cycle. Part II: assessment of NWP water budgets. *J Geophys Res* (in press)
- Moron V, Philippon N, Fontaine B (2004) Simulation of West African monsoon circulation in four atmospheric general circulation models forced by prescribed sea surface temperature. *J Geophys Res* 109:D24105. doi: [10.1029/2004JD004760](https://doi.org/10.1029/2004JD004760)
- Moufouma-Okia W, Rowell DP (2010) Impact of soil moisture initialisation and lateral boundary conditions on regional climate model simulations of the West African Monsoon. *Clim Dyn* 35:213–229. doi: [10.1007/s00382-009-0638-0](https://doi.org/10.1007/s00382-009-0638-0)

- Noilhan J, Planton S (1989) A simple parameterization of land surface processes for meteorological models. *Mon Weather Rev* 117:536–549
- Pohl B, Janicot S, Fontaine B, Marteau R (2009) Implication of the Madden–Julian oscillation in the 40-day variability of the West African monsoon. *J Clim* 22:3769–3785
- Ruti PM, Dell’ Aquila A (2008) The 20th century AEJ and AEWs in reanalyses and IPCC simulations. AMMA report
- Salas y Mélia D, Chauvin F, Déqué M, Douville H, Guérémy JF, Marquet P, Planton S, Royer J-F, Tyteca S (2005) Description and validation of CNRM-CM3 global coupled climate model, note de Centre du GMGEC 103, December 2005
- Separovic L, de Elia R, Laprise R (2008) Reproducible and irreproducible components in ensemble simulations with a regional climate model. *Mon Weather Rev* 136:4942–4961
- Seth A, Giorgi F (1998) The effects of domain choice on summer precipitation simulation and sensitivity in a regional climate model. *J Clim* 11:2698–2712
- Simmons A, Uppala SM, Dee D, Kobayashi S (2007) ERA-interim: new ECMWF reanalysis products from 1989 onwards. *ECMWF Newsl* 110:25–35
- Sperber KR, Palmer TN (1996) Inter-annual tropical rainfall variability in general circulation model simulations associated with the atmospheric model intercomparison project. *J Clim* 9:2727–2750
- Sultan B, Janicot S, Diedhiou A (2003) The West African monsoon dynamics. Part I: documentation of intraseasonal variability. *J Clim* 16:3389–3406
- Sylla MB, Coppola E, Mariotti L, Giorgi F, Ruti PM, Dell’ Aquila A, Bi X (2010) Multiyear simulation of the African climate using a regional climate model (RegCM3) with the high resolution ERA-interim reanalysis. *Clim Dyn* 35:231–247. doi:[10.1007/s00382-009-0613-9](https://doi.org/10.1007/s00382-009-0613-9)
- Uppala SM, Kallberg PW, Simmons AJ et al (2005) The ERA-40 reanalysis. *Q J R Meteor Soc* 131:2961–3012
- Vanvyve E, Hall N, Messenger C, Leroux S, van Ypersele JP (2008) Internal variability in a regional climate model over West Africa. *Clim Dyn* 30:191–202
- Wolter K, Timlin MS (1993) Monitoring ENSO in COADS with a seasonally adjusted principal component index. In: 17th climate diagnostics workshop, Norman, OK, pp 52–57
- Yoshimura K, Kanamitsu M (2008) Dynamical global downscaling of global reanalysis. *Mon Weather Rev* 136:2983–2998